Machine Learning-Based Autism Spectrum Disorder Classification Using an Enhanced Convolutional Neural Network Algorithm

P. Yugander[1], M. Jagannath[2]*
Research Scholar, School of Electronics Engineering, Vellore Institute of Technology, Chennai, Tamil Nadu, India [1]
Professor, School of Electronics Engineering, Vellore Institute of Technology, Chennai, Tamil Nadu, India [2]*

***Abstract*—Autism Spectrum Disorder (ASD) is a complex neurological developmental disability that appears during early childhood. Conventional ASD diagnostic techniques rely on behavioural observations, characteristics, and clinical interviews. To overcome these limitations, numerous machine learning (ML) and Deep Learning (DL) techniques have been used to assist physicians. For the past three decades, biomedical images have been employed to diagnose neurodevelopmental disorders. The functional Magnetic Resonance (MR) images used in this study. This paper proposes a novel machine learning framework to classify ASD control from healthy controls. The proposed framework consists of two stages. In the first stage, an enhanced Convolutional Neural Network (CNN) is proposed to extract features. In the second stage, the extracted features are given to the machine learning classifiers. The proposed method is tested on the 1112 fMRI images. A total of 539 ASD participants and 573 healthy controls are included in this study. A total of 17 datasets from the ABIDE website are used. These datasets are collected from various international medical laboratories. The proposed framework outperforms the existing methods. The proposed algorithm achieved 92.45% across the entire ABIDE dataset and 98.61% on the individual dataset.**

***Keywords*—Autism; enhanced CNN; random forest; MR images; logistic regression**

I. Introduction

Autism Spectrum Disorder (ASD) is a complex neurodevelopmental disorder that occurs in early childhood. It can be characterized by a person's social communication, interaction and behaviour. It is identified by the Autism Diagnostic Observation Schedule (ADOS), Autism Diagnostic Interview-Revised (ADI-R), the Diagnostic and Statistical Manual (DSM) of Mental Disorders and Computer-aided design (CAD) tools [1]. Among the above methods, ADOS is the gold standard for detecting ASD. However, CAD tools have become more popular in the last two decades. Numerous CAD tools are available to assist radiologists. With the help of CAD tools, radiologists can identify disease in its early stages and improve treatment [2]. It is a multidisciplinary technology that combines artificial intelligence with biomedical imaging techniques. It plays a vital role in diagnosing diseases like brain tumours, breast cancer, Alzheimer's disease, lung cancer, and autism [3]. Over the past two decades, there has been rapid growth in the prevalence of ASD. It has been identified that about 1 in 30 children lives in the USA. In addition, a larger number of researchers revealed that the prevalence of ASD in boys is four times higher than in girls [4]. X-ray imaging, computed tomography, magnetic resonance imaging, and fundus images are examples of biomedical images used by most researchers to identify and diagnose diseases [5]. These medical imaging techniques provide non-invasive views of the human body, enabling clinicians and researchers to image anatomy, identify abnormalities, and track disease progression across a broad range of conditions. However, CAD tools have become more popular in the last two decades. Functional MR images (fMRI) are used to identify functional connectivity between brain regions [6]. MRI is employed to examine the abnormalities of the brain. Compared to fMRI, sMRI is cost-effective. Clinicians use sMRI to identify autism using volumetric and geometric brain features [7]. It is used to detect brain morphological features due to its high spatial resolution and contrast sensitivity. Also, it does not use ionizing radiation, unlike other imaging techniques, which is especially important for adolescents and children. It contains different image sequences, such as T1, T2, and FLAIR. MR image analysis, feature extraction, and selection are significant challenges in biomedical image processing [8].

The above difficulties are overcome using ML and DL algorithms [9]. Classical ML algorithms such as SVM, RF, KNN, and LR are extensively used classifiers for ASD classification [10]. In addition, DL algorithms such as CNNs, Recurrent Neural Networks, Multilayer Perceptrons, Deep Belief Networks, and Long Short-Term Memory Networks have been used for ASD classification [11]-[13].

The multidimensional, high-complexity of fMRI data does not enable researchers to identify strong features that can discriminate between ASD and control groups. Repeated feature extraction techniques using fMRI data, engineered with simple ML algorithms, do not capture the complex neuroimaging patterns, resulting in poor classification results. More viable and dependable methods are needed to develop robust, more accurate ASD classification systems [14]. Traditional methods of ASD classification have used CNNs and 3D CNNs to extract spatial and temporal features from fMRI data. Nevertheless, these models perform poorly, especially when applied to multi-site datasets with varying imaging standards. The wide range of fMRI scanning protocols across institutions complicates the creation of models applicable across datasets [15].

TABLE I. SUMMARY OF THE PREVIOUS STUDIES

S.No	Study	Modality	Participants	Methods	Biomarkers	Accuray
1	Kong et al. 2018 [18]	fMRI	ASD = 78, NASD = 104	DNN	An abnormal cortical gray matter volume and cortical thickness found in ASD controls.	90.39%
2	Yang et al. 2022 [19]	fMRI	ASD = 505, NASD = 530	GCN	Distorted local and global neural patterns, as well as spatial and temporal controls, are observed in ASD controls.	75.9%
3	Mishra et al. 2023 [20]	sMRI	ASD=484 NASD=491	DCNN	The bilateral middle temporal gyri, orbitofrontal cortex, and insula have been observed in ASD controls.	81.35%
4	Irimia et al. 2018 [21]	sMRI	ASD=110 NASD=83	SVM	The ASD controls showed greater cortical thickness and white matter connectivity across more regions, including the frontal, temporal, and parietal lobes.	94.82%
5	Liu et al. 2025 [22]	fMRI	ASD= 539, NASD = 573	3D-CNN	ASD controls showed less functional connectivity between the rostral prefrontal cortex and the left cerebellum, and more between the right supramarginal gyrus and the middle temporal gyrus.	85%
6	Sabegh et al. 2023 [23]	fMRI	ASD= 539, NASD = 573	CNN	ASD has hyperconnectivity between the thalamus and the cerebral cortex that controls.	75.33%
7	Bahathiq et al. 2024 [24]	sMRI	ASD=311, TD=360	GWO-SVM	Higher cortical thickness across multiple frontal and temporal areas and higher subcortical volumes, including the putamen, pallidum, and amygdala, are observed in ASD controls.	71%
8	Jahani et al. 2024 [25]	sMRI	ASD= 351, NASD = 351	3D-DenseNet	Less gray matter volume and more gyrification were found in the temporal and frontal lobes in ASD controls.	76.9%
9	Reiter et al. 2019 [26]	fMRI	ASD= 306, NASD = 350	Random Forest	Increased cortical thickness in frontal and temporal areas, with reduced cortical thickness in parts of the cingulate and posterior areas, was found in ASD controls.	73.75%
10	Xu et al. 2024 [27]	sMRI	ASD= 40, NASD = 36	SVM	Increased thickness was observed in the superior frontal gyrus and the frontal pole of the ASD controls.	84.2%

Researchers need to develop sophisticated methods to analyze complex neuroimaging data while accounting for inherent data variability. The proposed study proposes an improved CNN to extract deep features, and ML classifiers, namely SVM, RF, KNN, and LR. The proposed ECNN architecture derives complex features from fMRI data, enabling ML classifiers to achieve high-accuracy classification of ASD. The suggested approach relies on an ECNN integrated with the conventional ML techniques [16].

The proposed framework evaluates its performance by analyzing the publicly available ABIDE-I dataset, which provides fusion data from 17 international sites for comprehensive model examination [17]. The experimental results confirm that the proposed framework achieves superior performance in ASD classification.

The structure of this paper is as follows: the previous literature survey is presented in Section II, the proposed method is explained in Section III, the Results are discussed in Section IV, and the conclusion and feature scope are given in Section V.

II. LITERATURE SURVEY

Katuwal et al. [28] have investigated 361 ASD controls and 373 healthy controls to identify ASD patients using sMR images. A random forest classifier is used to classify the ASD controls. Most abnormalities are found in ventricular, frontal, temporal, right hippocampal, and left amygdala regions. An AUC of 0.61 is achieved. The total of 734 samples is divided into subgroups based on age, autism severity, and Verbal IQ. The classification AUC increases to 0.92 by performing subgrouping. Zheng et al. [29] classified ASD controls using SVM classifiers. For this study, 66 high-functioning ASD controls and 66 healthy controls are used. The morphological features and multi-feature-based network features are given to SVM classifiers. This method produced a classification accuracy of 78.63%, with a sensitivity of 80% and a specificity of 77.27%.

Numerous researchers have used ML algorithms to identify structural abnormalities in patients with ASD. Structural abnormalities, such as total brain volume, subcortical volume, surface area and cortical thickness, are vital for identifying ASD

controls. Yassin et al. reported increased cortical thickness and decreased surface area in ASD controls. For this study, 36 ASD controls and 106 healthy controls were considered. The LR classifier achieved the highest accuracy among the remaining classifiers. The pathophysiologic findings of ASD are unclear yet, so the neuroanatomical features are considered a primary source for identifying ASD control from healthy controls. In addition, Xiao et al. [30] discriminated ASD controls from others using thickness-based, volume-based, and surface-area-based classification methods. They reported neuroanatomical abnormalities in the cortical surface, cortical thickness and cortical volume of ASD controls. They have used SVM, LR, RT, and KNN. Among the above ML algorithms, RT performed best. The random forest achieved the highest accuracy of 80.9%, sensitivity of 81.3%, and specificity of 81%. Table I presents the summarization of the different ASD identification methods with the use of both ML and DL algorithms.

III. Proposed Method

The proposed algorithm is tested on ABIDE website data, which is divided into ABIDE-I and ABIDE-II. Both datasets have sMRI, fMRI and Phenotypic data. A total of 17 datasets are available in ABIDE-1, and 19 datasets are available in ABIDE-II from various international medical laboratories. For this study, ABIDE-1 fMRI data are used. ABIDE-I contains 1112 subjects from 17 international datasets.

A. Data Preprocessing

Preprocessing MR image data is the most essential step in ASD classification. It enhances the validity and accuracy of the input data. The process involves two stages. In the first stage, skull stripping is performed. Disease identification is challenging for clinicians because of the complex brain structure and grey-level variations in MR images.

MRI image processing entails a fundamental set of pre-processing steps to clean, align, and enrich raw Blood Oxygen Level-Dependent (BOLD) signal data, with the aim of enabling accurate analysis. Such procedures will be necessary to eliminate noise, repair artefacts, and normalize data across subjects, enabling high-accuracy feature extraction and classification to distinguish cases of ASD from those of normally developing controls. All the steps take into account certain challenges in the acquisition of fMRI data and introduce the data to meaningful interpretation.

1) Skull stripping: This step involves removing non-brain tissue (e.g., the skull, scalp, and fat) from the images, leaving the brain parenchyma for analysis. Removing these extraneous structures, brain extraction reduces the dimensionality of the data and helps avoid non-neural signals from disrupting further processing. One can use tools like BET (Brain Extraction Tool) in FSL, AFNI 3dSkullStrip, or deep learning-based methods to create accurate brain masks that distinguish brain tissue from background.

2) Slice-timing correction: In functional MRI, volumes are recorded one slice at a time, and each slice is recorded at a slightly different time within the repetition time (TR). One technique to do this is to correct slice-timing to align all slices with a reference time, typically the midline slice, so that all voxels in a volume appear to be sampled simultaneously. This correction is essential for the correct modelling of the hemodynamic response and for the analysis of temporal dependence between brain regions, including studies of functional connectivity in ASD.

3) Motion correction: Subject motion during scanning is a major source of noise in fMRI data. Motion correction aligns all functional volumes to a reference volume (usually the first or middle volume) using rigid-body transformations. This procedure reduces the effect of head motion on BOLD signal measurements, especially in studies of ASD in children or individuals with limited ability to remain still during the scan. Framewise displacement is commonly computed to measure residual motion, and volumes with large motion can be labelled for later censure.

4) Distortion correction: Geometric distortions in fMRI images can be due to magnetic field inhomogeneities, especially at air-tissue interfaces such as the orbitofrontal cortex and temporal lobes. Fieldmap data is used to correct these distortions during the scanning session, providing an accurate spatial representation through the process of distortion correction. This step is commonly combined with motion correction to address both causes of spatial misalignment simultaneously, ensuring that BOLD signals are correctly localised to the regions where they are generated in the brain.

5) Registration: The functional images are not very sharp in spatial resolution or in tissue contrast, and it is hard to identify body structures directly from their functional images. Co-registration aligns the functional BOLD images with the subject's high-resolution structural T1-weighted image and enables accurate anatomical localisation of the subject's activation patterns. This alignment usually uses the registration algorithms that are based on the boundaries and which optimize the alignment between functional volumes and anatomical surfaces so that the signals can be properly attributed to a particular cortical and subcortical region.

6) Normalization: Brains vary widely in size and shape, making it difficult to compare them across subjects. Normalization maps each subject's images into a common template space, typically the MNI (Montreal Neurological Institute) template, using nonlinear transformations that account for individual anatomical differences. This step enables group-level analysis by aligning all brains to a common coordinate system, so that similar voxels indicate the same anatomical location across subjects. In children, templates should be age-specific and enhance registration accuracy.

7) Spatial smoothing: The normalized images are then passed through a Gaussian filter, which convolves each voxel's signal with those of its neighbours, effectively blurring the data. Spatial smoothing reduces high-frequency noise. It also helps explain anatomical variability among subjects after normalization. The kernel size is chosen based on the anticipated spatial extent of neural activation patterns.

8) Temporal filtering: fMRI time series have different frequencies of signal variations. The neural signature of interest

may be obscured by low-frequency noise, e.g., drift and physiological oscillations of the scanner, and by the high-frequency noise of the cardiac and respiratory cycles. Temporal filtering uses band-pass filters, usually keeping frequencies between 0.01Hz and 0.1Hz in resting-state fMRI to isolate activity fluctuations due to spontaneous neural activity and eliminate confounding noise. This is done to ensure that the time-series data used to extract features reflects actual changes in the BOLD signal rather than non-neural artefacts.

B. Transfer Learning Models

Transfer learning-based image classification is a popular method that uses pre-trained CNN models to improve model performance. These methods use pre-trained CNN models like Inception-V3, ResNet-50, DenseNet-121, and MobileNet-V3. Transfer learning-based models reduce the training time and improve neural network performance [31].

1) Inception-V3: It is a popular DL-based model used for image classification problems. It is the extended version of Inception-V2. It provides a lower error rate than Inception-V2. This model has forty-two input layers. It has been widely used for image classification applications for the past decade.

2) ResNet-50: Residual Network is a particular type of CNN. It builds the architecture using stacking residual blocks. It has forty-eight convolutional layers, a maximum pooling layer, and an average pooling layer. The ResNet-50 increases the feature extraction capability by incorporating the convolutional block attention module (CBAM). This CBAM increases feature extraction efficiency by learning spatial location information of the input data and channel information.

3) DenseNet-169: It is used to overcome the vanishing gradient problem in traditional CNN. Unlike CNN, all the layers in the DenseNet are connected using dense connectivity blocks. It contains a convolutional layer, a Max pooling layer, a dense layer, and transition layers. This model consists of Relu and SoftMax activation functions. DenseNet-169 architecture contains a varying number of layers and 4 Dens blocks. DenseNet-169 architecture reuses feature maps and reduces interdependence between layers by using dense blocks. Because of the above features, It provides high accuracy compared to the Resnet-121 and traditional CNN model [32].

4) MobileNet-V3: It was introduced primarily for mobile vision-related applications in 2017. Unlike CNN, it uses depthwise separable convolution (DSC) layers. Each DSC layer contains a depthwise convolution (DC) and a pointwise convolution (PC). A standard MobileNet-V3 has twenty-eight layers and four million parameters. It is the first mobile vision model of TensorFlow. This architecture splits each convolutional layer into a 3x3 DC layers and a 1x1 PC layer. It is also a lightweight neural network. Block diagram of the proposed method is shown in Fig. 1.

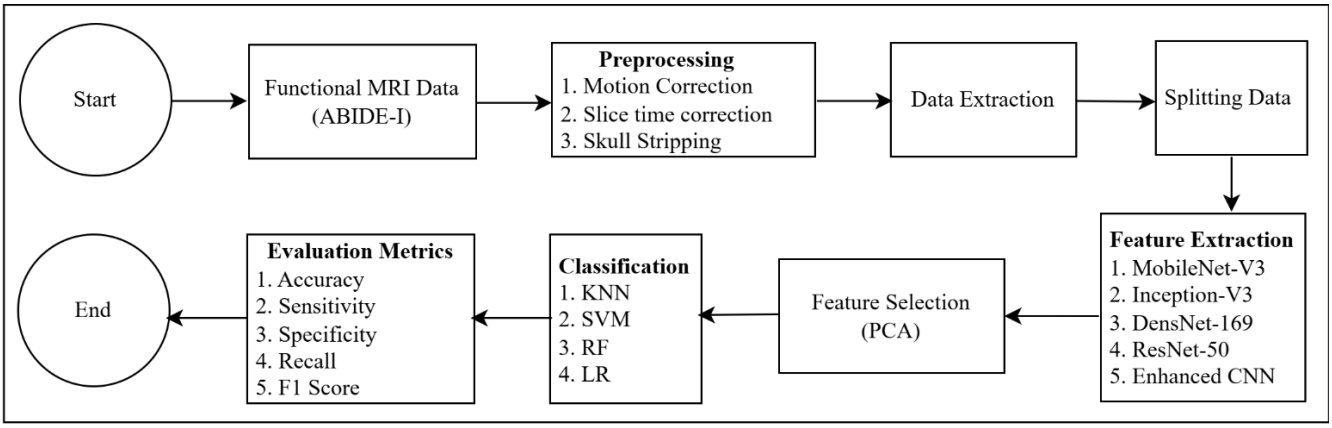

Fig. 1. Block diagram of the proposed machine learning framework.

C. Proposed Enhanced CNN

The proposed enhanced CNN model architecture is shown in Fig. 2. This ECNN architecture contains a convolutional layer (CL), LeakyRelu layer (LRL), max-pooling layer (MPL), dropout layer (DL), and batch normalization layer (BPL). The proposed algorithm is tested on 17 datasets from the ABIDE-1 website. The ABIDE-1 contains 539 ASD controls and 579 Healthy controls.

The input sMR images are data augmented to improve the performance of the ECNN model. In the ECNN model, the data size is considered 64. A total of 16 filters were used initially; these filters are doubled for the next layer. Finally, 256 filters are used in the last layer. The output of each layer varies dynamically. It can be eliminated by padding. By using padding, every output layer is equal to the channel input size. For this process, an alpha parameter is fixed to 0.1 and the MPL window size to 2x2. It is used to down sample the lRL output by choosing the maximum value from the 2x2 window. The most common problem in CNN is overfitting. The dropout layer is used to overcome the overfitting problem. We considered the dropout parameter to be 0.2. Finally, the fully connected layer flattens the data into one-dimensional space, and then the softmax layer produces the binary classification. In addition, principle component analysis (PCA) is used for feature selection.

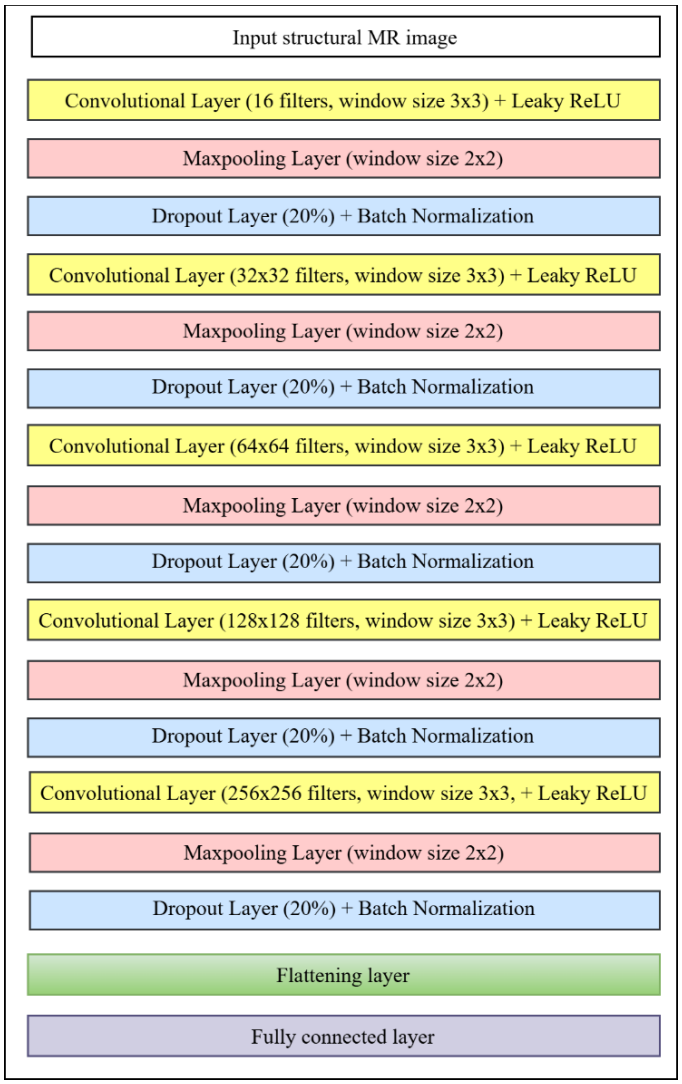

Fig. 2. Architecture of the proposed CNN model.

IV. Results and Discussion

For the past two decades, CNN has been widely used in biomedical image classification algorithms. In this paper, we have implemented the ML framework using an enhanced CNN model. The ABIDE-I dataset contains data from 17 international laboratories. It is tested on the entire 1112 sample and also tested on individual datasets.

The ABIDE-1 dataset is divided into two parts. One is used for training, and the other for testing. The training and testing split is 80:20. The training data is split into two parts: the first for training and the second for validation. The ROC curve, for a total of 1112 samples, is shown in Fig. 3. The accuracy curves and loss curves are shown in Fig. 4 to Fig. 5. The learning rate was fixed at 0.002 with a batch size of 16. The input is a 392x392 matrix, where each row corresponds to a different brain region in this enhanced CNN architecture. A total of 300 filters were used, ranging in size from 1x392 to 8x392. In general, dynamic-width filters are used in convolution. The connectivity matrix contains the correlation factor between various regions of the brain. The proposed algorithm is applied to 17 individual datasets. Among all datasets, the KKI dataset showed the highest accuracy. The ROC curve for the KKI dataset is shown in Fig. 6. The accuracy and loss curves are shown in Fig. 7 and Fig. 8, respectively.

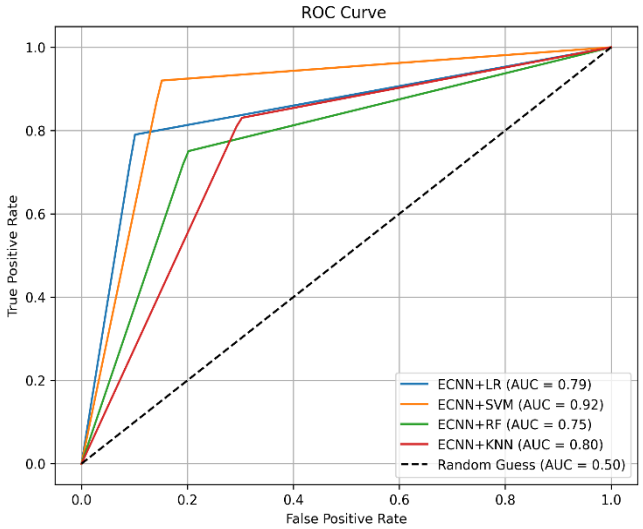

Fig. 3. ROC curve for entire ABIDE-1 data.

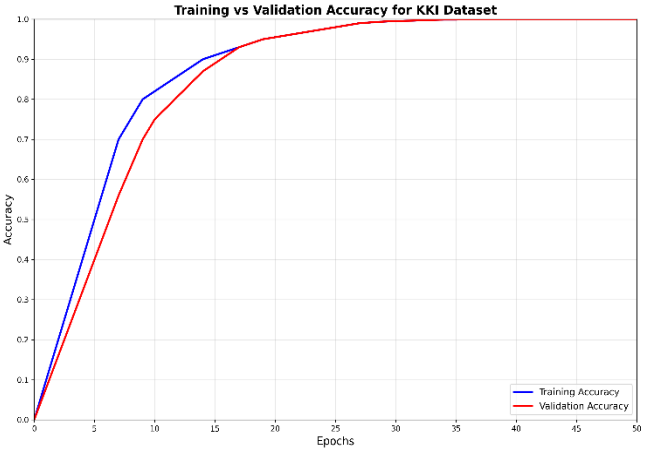

Fig. 4. Accuracy curve for ABIDE-1 data.

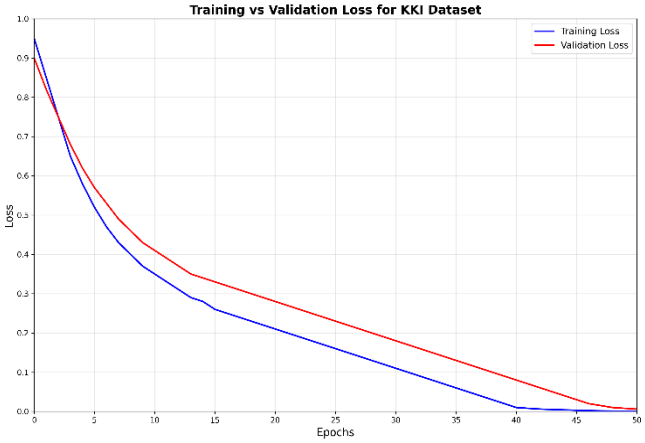

Fig. 5. Loss curve for ABIDE-1 data.

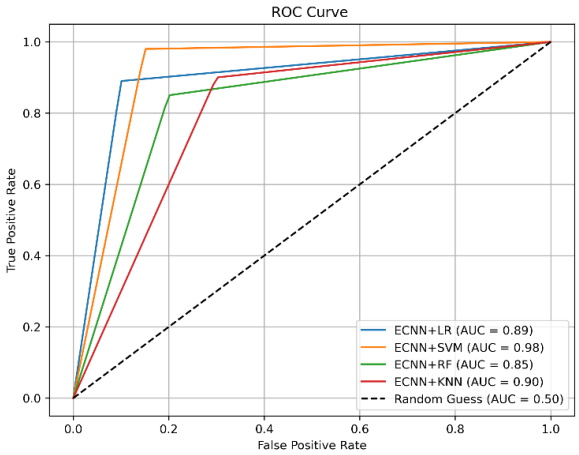

Fig. 6. ROC curve for KKI dataset.

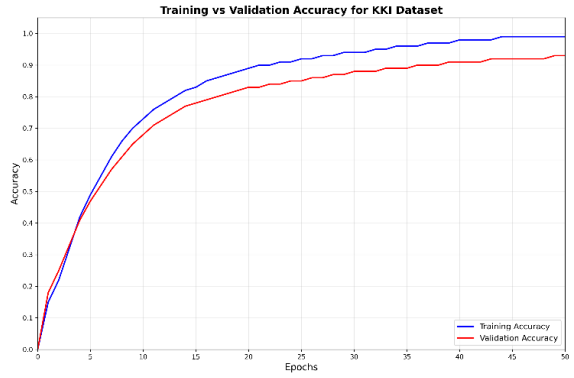

Fig. 7. Accuracy curve for KKI dataset.

The experimentation is done using windows 10 with Intel® Xeon® CPU E5-2420 @2.40GHZ, 15M Cache, 16GB RAM, NVIDIA GeForce RTX 3060, with 12 GB of memory. The proposed algorithm achieved higher AUC compared to other algorithms. The proposed ECNN algorithm is implemented using Python 3.12.2. The size of each row is equal to the dimension of the filter. Increasing the filter size does not increase the accuracy of the architecture.

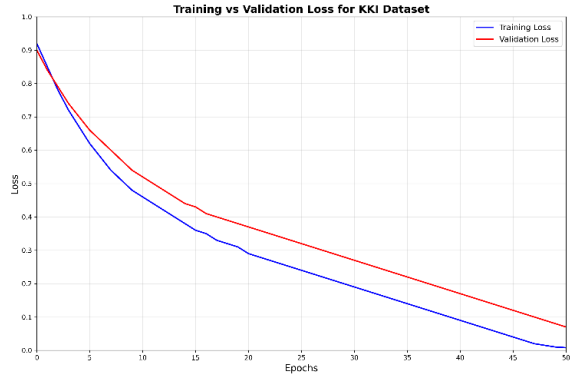

Fig. 8. Loss curve for KKI dataset.

In the first stage, we developed ECNN with several convolution layers concatenated. This proposed ML framework is compared with the existing algorithms. The results of the various algorithms are shown in Table II.

TABLE II. CLASSIFICATION RESULTS OF THE ENHANCED CNN ALGORITHM

Method	Accuracy (%)	Sensitivity (%)	Specificity (%)	Specificity (%)
Inception-V3	63.56	62.01	73.31	60.21
ResNet-50	69.78	61.23	60.02	72.11
DenseNet-169	70.45	68.21	71.89	67.77
MobileNet-V3	59.49	67.12	64.44	61.11
Proposed ECNN	72.44	69.01	77.01	74.43

TABLE III. CLASSIFICATION RESULTS OF THE PROPOSED ML FRAMEWORK FOR THE ENTIRE ABIDE-1 DATA

Method	Accuracy (%)	Sensitivity (%)	Specificity (%)	REC (%)
Inception-V3+KNN	70.64	73.53	88.33	81.11
Inception-V3+SVM	74.33	74.23	82.23	80.23
Inception-V3+LR	72.44	76.99	75.75	70.09
Inception-V3+RF	71.31	67.54	77.46	77.91
ResNet-50+KNN	75.11	89.22	69.44	81.90
ResNet-50+SVM	87.34	76.45	66.66	86.69
ResNet-50+LR	63.93	67.44	65.34	79.57
ResNet-50+RF	68.86	65.34	90.11	81.23
DenseNet-169+KNN	78.34	86.33	76.23	76.78
DenseNet-169+VM	77.32	79.34	75.54	81.45
DenseNet-169+LR	78.33	78.33	61.11	79.97
DenseNet-169+RF	81.36	87.67	67.33	76.45
MobileNet-V3+KNN	71.11	88.86	76.79	75.45
MobileNet-V3+SVM	87.22	76.32	81.88	78.89
MobileNET-V3+LR	67.44	71.11	79.11	76.54
MobileNet-V3+RF	74.33	85.19	73.98	71.98
ECNN+KNN	80.09	69.45	65.55	80.07
ECNN+SVM	92.45	91.43	92.22	89.56
ECNN+LR	79.11	77.87	78.35	69.96
ECNN+RF	75.22	74.77	76.59	70.01

The performance of the ECNN is evaluated in terms of Accuracy (ACC), Sensitivity (SEN), Specificity (SPC), and Recall (REC). The proposed ECNN showed the highest accuracy of 72.44%.

TABLE IV. CLASSIFICATION RESULTS OF THE PROPOSED ML FRAMEWORK FOR THE KKI DATASET

Method	Accuracy (%)	Sensitivity (%)	Specificity (%)	Specificity (%)
Inception-V3+KNN	75.04	75.36	91.43	71.51
Inception-V3+SVM	77.63	77.53	83.23	86.53
Inception-V3+LR	75.44	78.99	71.73	71.39
Inception-V3+RF	76.31	66.57	77.46	73.41
ResNet-50+KNN	77.71	87.27	69.94	85.90
ResNet-50+SVM	89.34	79.65	69.66	84.69
ResNet-50+LR	65.93	69.64	66.45	81.67
ResNet-50+RF	68.36	68.44	90.21	80.03
DenseNet-169+KNN	79.64	89.93	79.28	78.70
DenseNet-169+VM	76.32	81.34	79.44	84.44
DenseNet-169+LR	79.43	79.43	67.21	81.97
DenseNet-169+RF	91.36	67.67	87.33	86.45
MobileNet-V3+KNN	81.31	85.86	76.79	75.45
MobileNet-V3+SVM	77.22	76.32	71.87	77.79
MobileNET-V3+LR	69.94	81.31	76.11	78.54
MobileNet-V3+RF	76.34	82.34	78.88	81.08
ECNN+KNN	85.09	79.45	64.55	80.07
ECNN+SVM	98.61	93.43	95.22	89.56
ECNN+LR	89.11	79.87	73.26	69.96
ECNN+RF	85.22	75.77	79.98	70.01

Most researchers employed ML algorithms to classify ASD controls from healthy controls. These algorithms perform well

for small datasets. However, it could give better results for large datasets like ABIDE and NDAR. The proposed ML framework achieved 92.45% accuracy for the entire ABIDE-1 data and 98.61% accuracy for the individual Kennedy Krieger Institute (KKI) dataset. The summary of the various algorithms for the entire ABIDE-1 data is shown in Table III and the KKI dataset shown in Table IV.

TABLE V. PERFORMANCE COMPARISON

Study	Accuracy (%)	Dataset	Algorithm
Nafisah et al. [33]	73.50	ABIDE-1	SSDAE & MLP
Niu et al. [34]	73.20	ABIDE-1	DANN + Sigmoid
Eslami et al. [35]	80.00	ABIDE-1	Hypergraph Framework
Proposed ML framework	92.45	ABIDE-1	ECNN + SVM
	98.61	KKI	

The extracted features are given to the ML algorithm as input. These extracted features are given to the ML algorithms like SVM, KNN, RF and LR. The efficiency of the ML algorithms increased by the above process. The performance of the ML algorithm drastically improved by using ECNN extracted features. The proposed framework is compared to various existing algorithms. The comparison results are shown in Table V. The SVM classifier with ECNN performed well, with the highest accuracy of 92.45%. In the ABIDE database, 1,112 subjects were included in the total dataset. We used a 10-fold cross-validation approach to train and test our predictive model most rigorously, reducing the risk of overfitting and ensuring the generalizability of our findings. In this method, all participants (1,112) were randomly assigned to 10 equal groups (folds). The model was iteratively trained 10 times, with 9 folds (equivalent to about 1,001 subjects) used to train the model and the remaining fold (equivalent to about 111 subjects) used to validate the model. The final performance measures were then computed as the average across all 10 validation folds.

V. CONCLUSION

This paper proposed an ECNN and machine learning framework for classifying ASD controls from MR images. The proposed ECNN model is initially used to classify the ASD control from healthy controls. The proposed ECNN algorithm is tested on the ABIDE-I dataset. It performs well compared to existing CNN models. To improve the results, extracted features are given to the ML algorithms. The performance of the ML classifiers improved by using ECNN-extracted features. By combining the ECNN model and ML algorithms, we achieved high accuracy in classifying ASD and Healthy controls. This study contains two limitations. The first limitation is that we consider only fMR images. The proposed framework can be extended to sMR images in the future. The second limitation is that we considered only ABIDE-1 data. An ABIDE dataset contains ABIDE-I and II. It can be extended to ABIDE-II. Also, the proposed framework can be applied to 3D images.

REFERENCES

[1] R. K. Greene, I. Vasile,K. R. Bradbury, A. Olsen, and S. W. Duvall, "Autism Diagnostic Observation Schedule (ADOS-2) elevations in a clinical sample of children and adolescents who do not have autism: Phenotypic profiles of false positives," The Clinical Neuropsychologist, vol. 36, no. 5, pp. 943–959, Jul. 2022.

[2] O. Dekhil et al., "A Personalized Autism Diagnosis CAD System Using a Fusion of Structural MRI and Resting-State Functional MRI Data," Front Psychiatry. vol. 10, art no. 392, Jul. 2019.

[3] S. Neffati, K. Mekki, M. Machhout, "Deep learning-based CAD system for Alzheimer's diagnosis using deep downsized KPLS," Scientific Reports, vol. 15, no. 1, p.18556, May 2025.

[4] J. Duvekot et al., "Greaves-Lord K. Factors influencing the probability of a diagnosis of autism spectrum disorder in girls versus boys," Autism, vol. 21, no. 6, pp. 646-658, 2017.

[5] P. Yugander, K. Abhishek, P. S. Reddy, G. Manideep, T. Sahithi, and M. Jagannath, "Extraction of blood vessels from retinal fundus images using maximum principal curvatures and adaptive histogram equalization," In 2022 First International Conference on Electrical, Electronics, Information and Communication Technologies (ICEEICT), pp. 1-4, 2022.

[6] M. Akhavan Aghdam, A. Sharifi, M. M. Pedram, "Combination of rs-fMRI and sMRI data to discriminate autism spectrum disorders in young children using deep belief network," Journal of digital imaging. vol. 31, no. 6, pp. 895-903, Dec. 2018.

[7] M. Liu et al., "Diagnosis for autism spectrum disorder children using T1-based gray matter and arterial spin labeling-based cerebral blood flow network metrics," Front Neurosci, vol. 18, p.1356241, Apr. 2024.

[8] H. Alkahtani, T. H. Aldhyani, and M. Y. Alzahrani, "Deep learning algorithms to identify autism spectrum disorder in children-based facial landmarks," Applied Sciences, vol. 13, no.8, p. 4855, Apr. 2023.

[9] U Erkan and D. N. Thanh, "Autism spectrum disorder detection with machine learning methods," Current Psychiatry Research and Reviews Formerly: Current Psychiatry Reviews, vol. 15, no. 4, pp. 297-308, Dec. 2019.

[10] Y. Zhang, Y. Tian, P. Wu, D. Chen, "Application of skeleton data and long short-term memory in action recognition of children with autism spectrum disorder," Sensors, vol. 21, no.2, pp. 1-17, Jan. 2021.

[11] P. Yugander and M. Jagannath, "Classification of Autism Spectrum Disorder using Supervised Machine Learning Algorithms: A Review," in 2025 International Conference on Intelligent Computing and Control Systems (ICICCS), pp. 1291-1296, 2025.

[12] A. Lakhan, M. A. Mohammed, K. H. Abdulkareem, H. Hamouda, S. Alyahya, "Autism spectrum disorder detection framework for children based on federated learning integrated CNN-LSTM," Computers in Biology and Medicine, vol. 166, p. 107539, Nov. 2023.

[13] S. H. Sanjai et al., "Autism spectrum disorder detection using attention-based cnn and ml classifiers," Procedia Computer Science, vol. 258, pp. 4216-4227, 2025.

[14] T. Eslami, V. Mirjalili, A. Fong, A. R. Laird, and F. Saeed, "ASD-DiagNet: a hybrid learning approach for detection of autism spectrum disorder using fMRI data," Frontiers in neuroinformatics, vol. 13, p.70, Nov. 2019.

[15] J. Zhang, F. Feng, T. Han, X. Gong, F. Duan, "Detection of autism spectrum disorder using fMRI functional connectivity with feature selection and deep learning," Cognitive Computation, vol. 15, no. 4, pp. 1106-17, Jan. 2023.

[16] P. Yugander and M. Jagannath, "Autism Spectrum Disorder Detection using Enhanced 3D-ResNet50 Algorithm," SSRG International Journal of Electronics and Communication Engineering, vol. 13, no. 1, pp. 193-206, 2026.

[17] Di Martino et al., "The autism brain imaging data exchange: towards a large-scale evaluation of the intrinsic brain architecture in autism," Molecular psychiatry, vol. 19, no. 6, pp. 659-667, Jun. 2014.

[18] Y. Kong, J. Gao, Y. Xu, Y. Pan, J. Wang, and J. Liu, "Classification of autism spectrum disorder by combining brain connectivity and deep neural network classifier," Neurocomputing, 324, pp.63-68, 2019.

[19] T. Yang, M. A. Al-Duailij, S. Bozdag, and F. Saeed, F, "Classification of autism spectrum disorder using rs-fMRI data and graph convolutional networks," In 2022 IEEE International Conference on Big Data, pp. 3131-3138, 2022.

[20] M. Mishra and U. C. Pati "A classification framework for Autism Spectrum Disorder detection using sMRI: Optimizer based ensemble of deep convolution neural network with on-the-fly data augmentation," Biomedical Signal Processing and Control, 84, p.104686, 2023.

[21] A. Irimia et al. "Support vector machines, multidimensional scaling and magnetic resonance imaging reveal structural brain abnormalities associated with the interaction between autism spectrum disorder and sex," Frontiers in computational neuroscience, vol. 12, p.93, 2018.

[22] Z. Liu, Y. Chen, X. Dong, and J. Liu, "An Autism Spectrum Disorder Identification Method Based on 3D-CNN and Segmented Temporal Decision Network," Brain Sciences, vol. 15, issue. 6, p.569, 2025.

[23] A. M. Sabegh, N. Samadzadehaghdam, H. Seyedarabi, and T. Ghadiri, "Automatic detection of autism spectrum disorder based on fmri images using a novel convolutional neural network," Research on Biomedical Engineering, vol. 39, issue. 2, pp. 407-513, 2023.

[24] R. A. Bahathiq, H. Banjar, S. K. Jarraya, A. K. Bamaga, R. Almoallim, "Efficient diagnosis of autism spectrum disorder using optimized machine learning models based on structural MRI," Applied Sciences, vol. 14, issue. 2, p. 473, 2024.

[25] A. Jahani et al. "Twinned neuroimaging analysis contributes to improving the classification of young people with autism spectrum disorder," Scientific reports, vol. 14, p.20120, 2024.

[26] M. A. Reiter, A. Jahedi, A. J. Fredo, I. Fishman, B. Bailey, and R. A. Muller, "Performance of machine learning classification models of autism using resting-state fMRI is contingent on sample heterogeneity," Neural computing and applications, vol. 33, issue. 8, pp.3299-3310, 2021.

[27] X. Xu et al. "Quantitative assessment of brain structural abnormalities in children with autism spectrum disorder based on artificial intelligence automatic brain segmentation technology and machine learning methods," Psychiatry Research: Neuroimaging, vol. 345, article no. 111901, 2024.

[28] G. J. Katuwal, S. A. Baum, N. D. Cahill and A. M. Michale, "Divide and conquer: sub-grouping of ASD improves ASD detection based on brain morphometry", Plos One, vol. 11, no. 4, Apr. 2016.

[29] W. Zheng, T. Eilam-Stock, T. Wu, "A Spagna, C Chen, B Hu and J Fan, "Multi-feature based network revealing the structural abnormalities in autism spectrum disorder", IEEE Transactions on Affective Computing, vol. 12, no. 3, pp. 732-742, Jan. 2019.

[30] X. Xiao, et al., "Diagnostic model generated by MRI - derived brain features in toddlers with autism spectrum disorder", Health Information Science and Systems, vol. 7, no. 1, Apr. 2017.

[31] X. Di and B. B. Biswal, "A functional MRI pre-processing and quality control protocol based on statistical parametric mapping (SPM) and MATLAB," Frontiers in Neuroimaging, pp. 1-12, Jan. 2023.

[32] P. Yugander, K. Sneha, C. S. Raju, J. Sunny, T. Revanth, and M. Jagannath. "Autism Spectrum Disorder Classification Using a Hybrid Deep Learning Framework," In 2025 International Conference on Computing Technologies & Data Communication (ICCTDC),pp. 1-5, 2025.

[33] I. Nafisah et al., "Deep learning-based feature selection for detection of autism spectrum disorder," Frontiers in Artificial Intelligence, vol. 8, p.1594372, Jun. 2025.

[34] K. Niu et al., "Multichannel deep attention neural networks for the classification of autism spectrum disorder using neuroimaging and personal characteristic data," Complexity, vo. Jan. 2020.

[35] T. Eslami, V. Mirjalili, A. Fong A, A. R. Laird and F. Saeed, "ASD-DiagNet: a hybrid learning approach for detection of autism spectrum disorder using fMRI data," Frontiers in neuroinformatics, vol. 13, artcile no. 70, 2019.